

## Article

# A New Cloud-Based IoT Solution for Soiling Ratio Measurement of PV Systems Using Artificial Neural Network

Mussawir Ul Mehmood <sup>1</sup>, Abasin Ulasyar <sup>1,\*</sup>, Waleed Ali <sup>1</sup>, Kamran Zeb <sup>2</sup>, Haris Sheh Zad <sup>3</sup>,  
Waqar Uddin <sup>4</sup> and Hee-Je Kim <sup>5,\*</sup>

<sup>1</sup> Department of Electrical Power Engineering, USPCAS-E, National University of Sciences and Technology (NUST), Islamabad 44000, Pakistan

<sup>2</sup> School of Electrical Engineering and Computer Science, National University of Sciences and Technology (NUST), Islamabad 44000, Pakistan

<sup>3</sup> Department of Mechanical and Manufacturing Engineering, Pak-Austria Fachhochschule, Institute of Applied Sciences and Technology, Haripur 22620, Pakistan

<sup>4</sup> Department of Electrical Engineering, National University of Technology, NUTECH, Islamabad 44000, Pakistan

<sup>5</sup> School of Electrical Engineering, Pusan National University, Pusandaehak-ro 63 beon-gil 2, Geumjeong-gu, Busan 46241, Republic of Korea

\* Correspondence: abasin@uspcase.nust.edu.pk (A.U.); heeje@pusan.ac.kr (H.-J.K.)

† All the future correspondence regarding this article should be directed to Abasin Ulasyar.

**Abstract:** Solar energy is considered the most abundant form of energy available on earth. However, the efficiency of photovoltaic (PV) panels is greatly reduced due to the accumulation of dust particles on the surface of PV panels. The optimization of the cleaning cycles of a PV power plant through condition monitoring of PV panels is crucial for its optimal performance. Specialized equipment and weather stations are deployed for large-scale PV plants to monitor the amount of soil accumulated on panel surface. However, not much focus is given to small- and medium-scale PV plants, where the costs associated with specialized weather stations cannot be justified. To overcome this hurdle, a cost-effective and scalable solution is required. Therefore, a new centralized cloud-based solar conversion recovery system (SCRS) is proposed in this research work. The proposed system utilizes the Internet of Things (IoT) and cloud-based centralized architecture, which allows users to remotely monitor the amount of soiling on PV panels, regardless of the scale. To improve scalability and cost-effectiveness, the proposed system uses low-cost sensors and an artificial neural network (ANN) to reduce the amount of hardware required for a soiling station. Multiple ANN models with different numbers of neurons in hidden layers were tested and compared to determine the most suitable model. The selected ANN model was trained using the data collected from an experimental setup. After training the ANN model, the mean squared error (MSE) value of 0.0117 was achieved. Additionally, the adjusted R-squared ( $R^2$ ) value of 0.905 was attained on the test data. Furthermore, data is transmitted from soiling station to the cloud server wirelessly using a message queuing telemetry transport (MQTT) lightweight communication protocol over Wi-Fi network. Therefore, SCRS depicts a complete wireless sensor network eliminating the need for extra wiring. The average percentage error in the soiling ratio estimation was found to be 4.33%.

**Keywords:** internet of things; solar energy; solar efficiency; cloud; edge device; machine learning



**Citation:** Ul Mehmood, M.; Ulasyar, A.; Ali, W.; Zeb, K.; Zad, H.S.; Uddin, W.; Kim, H.-J. A New Cloud-Based IoT Solution for Soiling Ratio Measurement of PV Systems Using Artificial Neural Network. *Energies* **2023**, *16*, 996. <https://doi.org/10.3390/en16020996>

Academic Editor: Hai Lan

Received: 29 November 2022

Revised: 4 January 2023

Accepted: 11 January 2023

Published: 16 January 2023



**Copyright:** © 2023 by the authors. Licensee MDPI, Basel, Switzerland. This article is an open access article distributed under the terms and conditions of the Creative Commons Attribution (CC BY) license (<https://creativecommons.org/licenses/by/4.0/>).

## 1. Introduction

Around 75% of the world's fossil fuel consumption is used to generate heat and electricity [1]. The extensive use of fossil fuels is damaging to the environment. The burning of conventional fossil fuels, such as coal, natural gas, and petrochemicals, release toxic gases and chemicals into the environment, causing land and air pollution. The resulting pollution from burning of fossil fuels is the major cause of global warming and the

health problems that negatively affect human life [2]. In addition to the environmental and health concerns, fossil fuels are also limited in supply. Since fossil fuels are non-renewable, their complete depletion should be avoided, in order to preserve these resources for future generations. It is estimated by some experts that at the current rate of consumption, oil and gas reserves will decrease to 14% and 18%, respectively, by the end of year 2050 [3]. All of the above-mentioned issues have forced governments all over the world to look for alternative clean and renewable energy sources. Therefore, the adoption of renewable energy is on the rise all over the world. This trend is expected to accelerate over the coming years. Out of all the available renewable energy sources, solar energy, or the energy harvested from solar radiation, is the most abundant form of energy. The surface of earth receives solar radiation at an average rate of  $343 \text{ W/m}^2$ . Ref. [4] presented a study to assess the potential of solar photovoltaic power generation in China. The results show that China has potential to generate 131.942 PWh of energy by using solar radiation. This value is approximately 23 times the overall electrical energy demand of China. Solar radiation is directly converted to electrical energy by using photovoltaic (PV) systems [5,6].

The efficiency of PV panels is affected by environmental conditions. One of the main causes of degradation of PV panel is soil or dust accumulation on the surface [7,8]. Soiling induces transmittance losses in PV panels. Transmittance loss causes a decrease in the power generation from PV panels. Reduction of the soiling in PV systems has been one of the major topics in PV systems research and development [9–11]. Ref. [12] presented an experimental work to study the effects of soiling on PV efficiency. A maximum transmittance loss of 69.06% and a power loss of 29.76% were recorded during dry period encountering no rain. In addition to this, accelerated soiling can also occur due to unusual environmental conditions. These environmental conditions rapidly decrease PV panel efficiency if regular cleaning is not performed. A study was presented in [13], where panels were placed near a construction site, and the soiling of PV panels was recorded. It was found that the PV system output efficiency was reduced to an alarming value of 20% within a period of 5 months. Similarly, a detailed study was presented in [14], highlighting the effects of soiling on PV modules deployed at five different locations. To reduce the effect of soiling and to achieve maximum efficiency, PV panels need to be regularly monitored to calculate the amount of dust accumulated. It is challenging to experimentally study the soiling losses in PV plants everywhere because of the ever-changing environmental conditions. As the world is moving towards solar energy, people are giving more attention to accurate soiling loss modeling over time [15]. Generally, PV plants use dedicated soiling stations to monitor and reduce the effects of soiling [16]. A soiling station is used to help operators determine when and where the PV panels require cleaning. A soiling station does not provide a physical measurement of the dust and particulates on the actual PV panels. Rather, it is used as a reference point to understand what percentage of power loss is due to soiling. It provides a value that represents the amount of soiling on the surface of the PV panel.

The soiling station-based method can be broadly divided into two categories: (i) Optical measurement-based methods; (ii) electrical parameter measurement-based methods. Optical-based methods utilize digital imagery or measurement of light reflection from reference reflective surface to approximate amount of soiling. An aerial imaging method was proposed in [17] to quantify soiling on PV panels. This method used a metric called the black and white ratio to calculate the soiling on proxy surfaces. However, the results were dependent on camera settings and imaging conditions, which may vary significantly from one location to another. Ref. [18] proposed a novel soiling detection scheme by using an image entropy technique on a reference piece of plasticized paper mounted alongside a PV panel. Similarly, some electrical parameter measurement-based soiling detection kits are available for large-scale PV installations [19,20]. However, these solutions are often available as part of complete and specialized weather stations, and are not suitable for small- and medium-scale PV plants because of cost constraints. Additionally, the majority of the PV soiling stations require two PV modules placed adjacent to each other under the

same physical and environmental conditions [21]. One of the modules is required to be cleaned regularly, in order to provide reference parameters, which are then compared to the parameters obtained from the soiled panel to determine the soiling ratio. Electrical parameters (short circuit current, power output) are measured for both panels and compared to the approximate soiling loss.

A new cost-effective and scalable solution is required that can be integrated with small-, medium-, and large-scale PV plants. The recent advancements in technologies such as artificial neural networks (ANN), IoT, and cloud computing have made the deployment of cost-effective and scalable systems possible [22,23]. This is achieved by integrating technologies such as artificial neural networks (ANN) [24,25] and IoT [26,27]. Artificial neural networks have already found applications in the field of renewable energy [28,29]. ANNs are extensively used in the area of energy generation and consumption forecasting [30]. A deep learning-assisted framework AB-Net uses a combination of an auto-encoder and bidirectional long short-term memory algorithms for short-term one-step forecast of renewable energy generation [31]. Short-term energy production is helpful in efficient trading, integration, storage management, and control systems for renewable energy systems. Similarly, ANNs can be used to predict the amount of soiling on the surface of PV panels, in order to optimize cleaning cycles, hence boosting the efficiency of PV plants and renewable energy generation. Therefore, authors have proposed a complete centralized soiling detection system based on IoT and ANN that requires only one PV panel per soiling station to operate. In the proposed system, clean or reference panel is replaced by ANN. The ANN model is trained to predict the short circuit current ( $I'_{sc}$ ) of the clean PV panel by using the electrical and environmental parameters of the soiled panel, which is then compared to the short circuit current obtained from the soiled panel ( $I_{sc}$ ) to approximate the soiling, therefore eliminating need for the clean PV panel altogether. The advantage of this scheme is twofold: not only to eliminate one physical panel, but also to eliminate the need to regularly clean the reference panel. This research work presents a cloud-based centralized solution for monitoring soiling losses. The ANN algorithm used for soiling loss measurement is hosted on a cloud server. The benefit of this type of centralized scheme is that all the processing required is performed on a centralized server. This reduces the complexity of the equipment used in the soiling station, as it only needs to measure and transmit the parameters to the server. IoT provides the communication infrastructure between the sensors and cloud server. The main contributions of this research work are as follows:

- SCRS uses the least number of input parameters, when compared to other techniques used in the available literature. Only three parameters are required by SCRS to estimate the soiling ratio. SCRS uses environmental and electrical parameters to detect soiling that can be obtained using low-cost sensors and microcontroller. This helps with the further reduction of the overall cost required for the detection of soiling losses per unit area of PV panels.
- Traditional methodology found in the literature requires two panels to monitor soiling, one of which is cleaned regularly to provide reference parameters for soiling detection. We have presented a new and simplified design of a soiling station by replacing the reference panel with the ANN model. The model was trained to predict the short circuit current of the reference panel by using the environmental and electrical characteristics of the soiled panel. The predicted short circuit current and actual short circuit current of the soiled panel are used to calculate the soiling ratio.
- A centralized cloud-based architecture [32] was introduced to further reduce the cost and complexity of the equipment used in soiling stations. IoT architecture was introduced to make the system scalable and more accessible by offloading the processing and communication infrastructure to a cloud server. Google cloud services were used in the proposed system. A microcontroller-based Wi-Fi capable communication module was used to communicate to the internet gateway device. This increases the reliability of the system, as additional wiring is not required and eliminates the cost infrastructure required for the wired connection for each soiling station. The lightweight

Internet of Things protocol (MQTT) was used to define the message format between the soiling stations and cloud server. MQTT has become the industry standard because of the low packet overhead and user customization feature set, as compared to protocols such as Hypertext Transfer Protocol (HTTP) [33,34]. Additionally, the implementation of centralized cloud-based architecture allows multiple SCRS systems to share cloud computing resources.

The rest of the paper is structured as follows: An overview of the proposed system is presented in Section 2. Section 3 explains the IoT architecture. The experimental setup for data collection is provided in Section 4. Section 5 presents the results and discussion. Section 6 includes the limitation and future work. Finally, the conclusion is provided in Section 7.

## 2. Solar Conversion Recovery System (SCRS) Overview

Figure 1 shows the proposed system for the detection of soiling ratio. As shown in the diagram, SCRS relies only on one PV panel to predict the soiling ratio. SCRS comprises of two main components: (i) the performance measuring cabinet (PMC) and (ii) cloud server. PMC is a weatherproof enclosure that houses all the electronic equipment. Different sensors measure the performance parameters (short circuit current ( $I_{sc}$ ), light intensity (L), open circuit voltage ( $V_{oc}$ ), and temperature (T)) of the PV panel at regular intervals. “NodeMCU”, an open source IoT platform [35], acts as edge device and collects the performance parameters. The edge device sends performance parameters to a centralized cloud server instance hosted at Google cloud services. The cloud server hosts the ANN algorithm that is responsible for the prediction of the reference parameter ( $I'_{sc}$ ). ANN uses electrical and environmental parameters to predict  $I'_{sc}$ . The actual short circuit current ( $I_{sc}$ ) of the soiled panel and the predicted short circuit current ( $I'_{sc}$ ) are used to calculate the soiling ratio (SR), according to Equation (1).

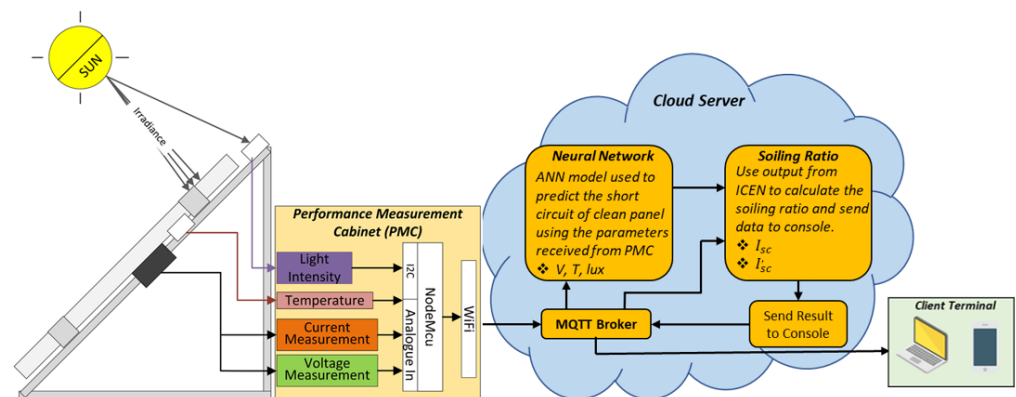


**Figure 1.** SCRS components and block diagram.

The SR value is then transmitted for visualization at the control center using MQTT. Figure 2 shows the proposed IoT architecture for the SCRS. The initial stage of the IoT system is the perception layer. The main objective of this layer is to bridge the real and digital worlds. The perception layer would host PV panels with attached sensors. The real-world analogue signals are converted to digital format in this layer. Digital signals are then handed over to the next layer for transmission. The second layer in this architecture is network layer or communication layer. This layer oversees all the communication between the devices, networks, and cloud that make up the entire IoT system. The edge device is used in this layer to communicate sensor information from physical devices to data centers. Additionally, some intelligence can be added to the edge device to make context-aware decisions based on the data from perception layer [36]. While both wired and wireless com-

munication technologies can be used, IoT systems generally rely on wireless technologies, as they are easier and more cost-effective to deploy in distributed environments.

$$SR = \frac{I_{sc}}{I'_{sc}} \quad (1)$$

In the proposed architecture of Figure 1, “Node MCU” is used as the edge device in network layer [37,38]. Furthermore, edge intelligence has been added by using a real-time clock (RTC) module. The edge device uses RTC to keep track of the time and transmit data only during the specified time intervals. The middleware layer can be considered as the brains of IoT system, as it contains the most intelligent and high resource components mainly responsible for the accumulation, storage, and processing of the data received from the previous layer. This layers also holds the data messaging tools that define the format of the messages exchanged between various components of the IoT system. While there are many protocols available for IoT messaging, we have used MQTT as the messaging protocol. MQTT is a light weight publish and subscribe messaging protocol specially built for IoT applications, and it works well even for constrained networks. Ref. [39] presented a study on various IoT messaging protocols. It was found that MQTT is the most suitable protocol for cloud-based applications. After processing the data in the middleware, the results are sent to the application layer where stakeholders can visualize the data and interact with the system. The application layer comprises of user interfaces, such as mobile applications, browser-based applications, or other visualization tools. The application layers can allow stakeholders to change the operational parameters of the system at run-time, such as changing the data reporting frequency of edge devices.

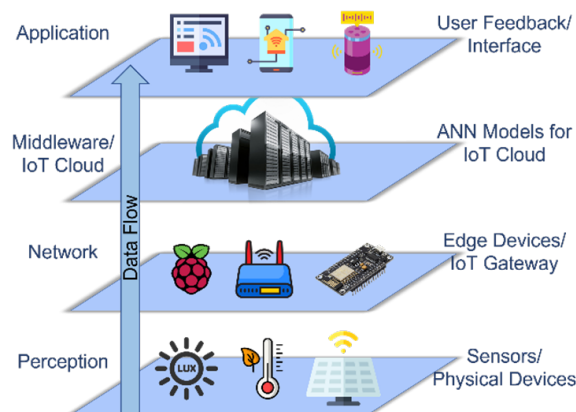


Figure 2. An IoT-based architecture for soiling detection system.

### 3. ANN Architecture Selection and Data Collection for Machine Learning

ANNs are powerful mathematical frameworks. The robustness of these models is manifested in the modeling of very complex systems, for which the analytical modeling is not possible. For this reason, ANNs have been vastly used for a variety of applications in the last three decades [40–42]. ANNs are inspired by biological functioning of human brain. They consist of some number of neurons interconnected to each other, as shown in Figure 3. A single neuron can have one or more inputs ( $x_n$ ), and each input is assigned a weight ( $w_n$ ).

These weights are fixed during testing, but these numbers can change during the training process to “tune” the ANN. A neuron consists of two parts; first is the linear combination of the inputs and weights, as defined in Equation (2), and the second part consists of a nonlinear activation function [43]. The rectified linear unit (ReLU) was used in the proposed neural network because of its faster convergence rates and reduced likelihood of vanishing gradients [44], as shown in Equation (3). Thus, the output  $F(X)$  of a neuron, as shown in Figure 3, can be defined with Equation (4).

$$f(X) = b_1 + x_1w_1 + x_2w_2 + \dots + x_nw_n \quad (2)$$

$$\text{ReLU}(x) = \max(0, x) \quad (3)$$

$$F(X) = \max(0, b_1 + x_1w_1 + x_2w_2 + \dots + x_nw_n) \quad (4)$$

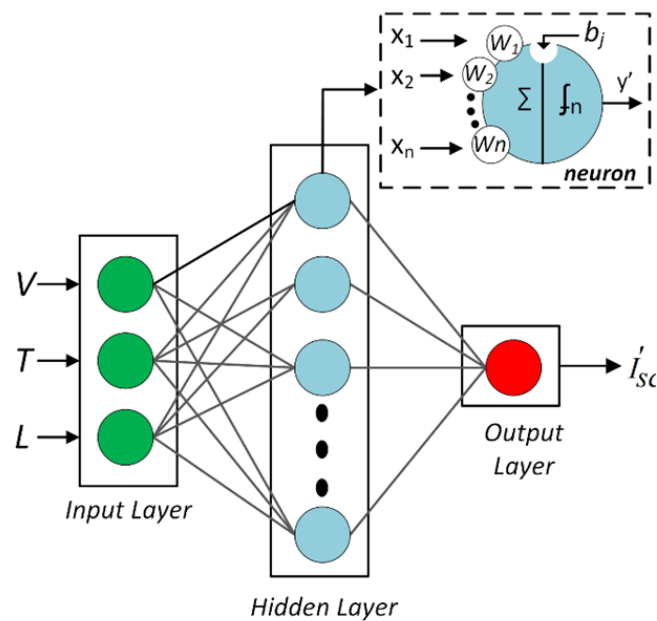


**Figure 3.** Architecture of proposed ANN model.

The ANN architecture is divided into three main parts: an input layer, the hidden layers, and an output layer. The ANN model used in this work is composed of one input layer, one hidden layer, and one output layer. The maximum number of epochs was set to 1000. Early stopping was enabled with a patience parameter of value 10. The batch size was selected equal to 32. “RMSprop” was used as an optimizer, and the learning rate was set to  $1 \times 10^{-3}$ .

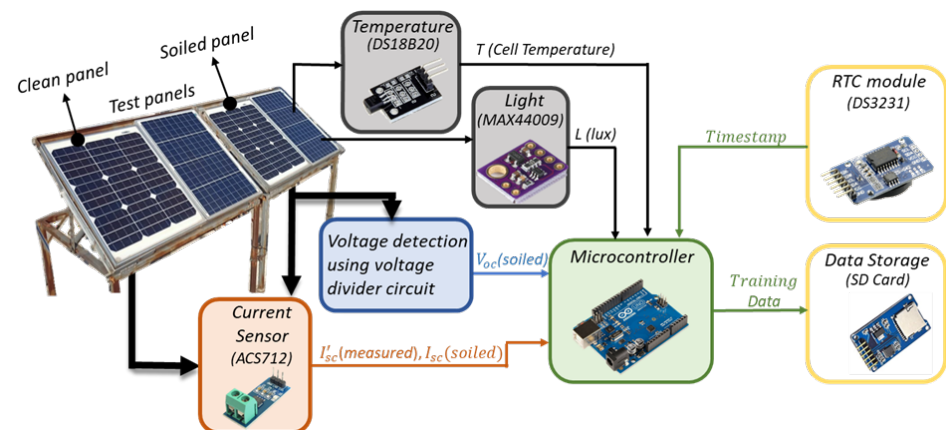
An ANN with one hidden layer presents a simpler computation and lower weight error propagation [45,46]. The input layer was composed of three input features shown in Table 1. The dataset was randomly divided into 80% for training, and 20% for validation and testing. To collect the training data, outdoor experiments were conducted at National University of Sciences and Technology, Islamabad, Pakistan campus. A testbed was installed as shown in Figure 4. During the data collection stage, clean and soiled panels were installed side-by-side under same environmental conditions. The data were collected at 5 min intervals for a period of 2 months. Each set of measurements were stored with timestamps. Only the data recorded between 7:00 am and 7:00 pm were used for each day. A summary of the parameters recorded is presented in Table 1. Notice that the input parameters have significantly varying ranges, as evident from the maximum and minimum values. Training data with varying ranges can cause a slower convergence and biased training due to very large or small weights [47,48]. Therefore, the input parameters were normalized between 0 and 1 by using the min-max normalization, which is given by Equation (5).

$$x_i = \frac{x - x_{min}}{x_{max} - x_{min}} \quad (5)$$

where  $x_i$  represents the normalized value of feature  $x$ ,  $x_{min}$  represents the minimum value of the feature vector, and  $x_{max}$  represents the maximum value of the feature vector.

**Table 1.** Summary of parameters collected for training process of artificial neural network.

Parameter	Min	Max	Unit
Input parameters for neural network			
Open circuit voltage of soiled panel (V)	11.97	24.1	Volts
Cell temperature (T)	25.62	64.12	°C
Light intensity (L)	1152	77,783	lux
Output labels for neural network			
Short circuit current of clean panel ( $I_{sc\_clean}$ )	0	1.61	Ampere

**Figure 4.** Hardware setup for collection of training data for artificial neural network used in SCRS.

#### 4. Experimental Setup

An experimental setup was built to validate the performance of SCRS. Operational block diagram of the experimental setup is shown in Figure 5. Jinko Solar 270 W photovoltaic panel is deployed in this experiment, with the PMC containing electronic circuitry for data acquisition. In order to measure temperature and light intensity, DS18B20 digital temperature sensor and max44009 ambient light sensors are used. ACS712 current sensor and a voltage divider is used to measure current and voltage of the PV panel. Note that we are using ambient light intensity, instead of solar insolation, as data input to the neural network. This approach was used to keep the cost of SCRS low, as the ambient light intensity can be measured using low-cost sensors, such as max44009. Jinko 270 Watt PV panels were used with maximum power current and maximum power voltage values of 8.52 A and 31.7 V, respectively. The PV panels were placed on an angle of 40° with a horizontal plane. A relay module was used to switch between the voltage-measuring circuit and the current-measuring circuit. The sensors are connected to NodeMCU which is a low-cost Wi-Fi capable micro-controller, as shown in Figure 6. To compensate for the unavailability of analog-to-digital converter (ADC) channels on NodeMCU, an ADS1115 analog-to-digital converter module is used to convert analog current and voltage readings to 16-bit digital format. The RTC module is used to keep track of time.

The RTC module enabled the micro-controller to transmit sensor data only during the daylight hours. The sensor data is encoded using javascript object notation (JSON), a lightweight format for storing and transporting data. Encoding can be described as a given sequence of characters or converting the data, into a specified format, for secured transmission of data. On the other hand, decoding is the reverse process of encoding, which is used to extract the information from the converted data. The data is transmitted between devices using the MQTT protocol. The cloud server waits for the data arriving from NodeMCU. The ANN model uses the sensor information to estimate  $I'_{sc}$ . At the end, the soiling ratio is calculated using Equation (1). The results are transmitted to the client

application available at the monitoring station. The client application was built in the .NET Framework using the C# programming language.

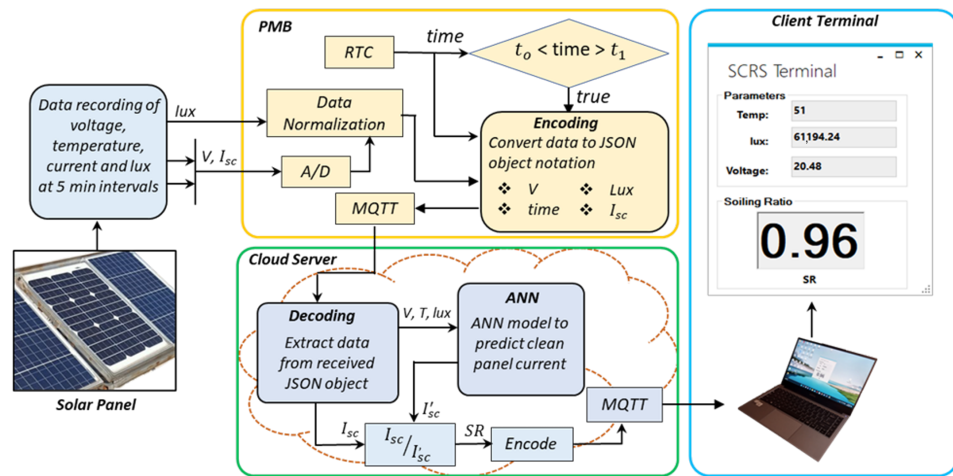


Figure 5. Operational block diagram of solar conversion recovery system (SCRS).

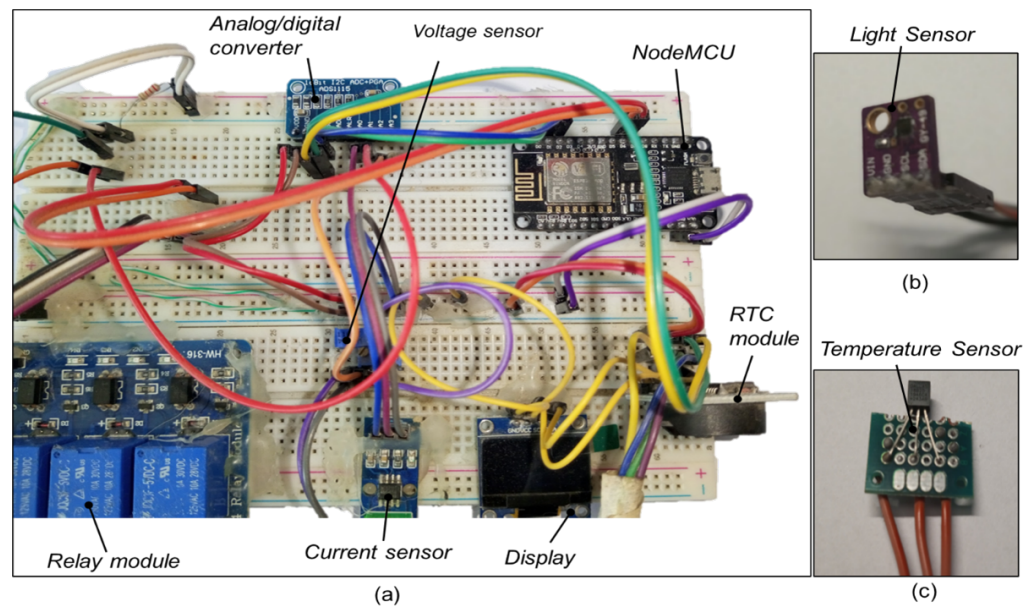


Figure 6. (a) Electrical circuit for SCRS placed in performance measurement box. (b) Light intensity sensor. (c) Digital temperature sensor.

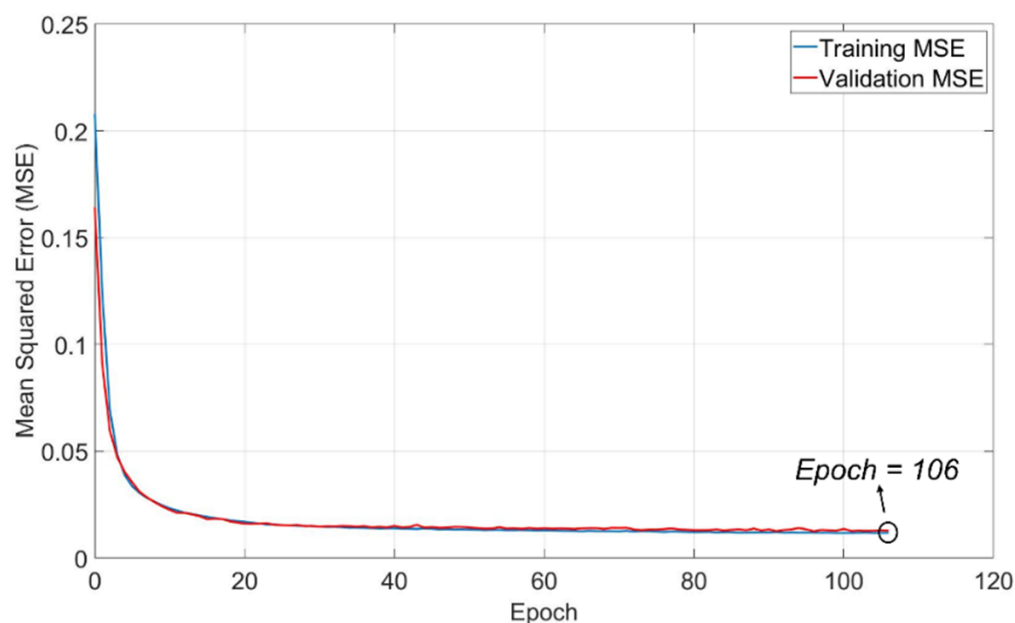
### 5. Results and Discussion

One of the important parameters in ANN model design is the choice of the number of training epochs to use. A large number of epochs can lead to the over-fitting of training data, whereas too few may result in an under-fitting model. To avoid over-fitting or under-fitting conditions, the “Early stopping” feature was used. The early stopping feature automatically stops the training process once the model performance stops improving on the validation dataset. Multiple ANN models were tested by varying the number of neurons between 5 and 35 in increments of 10, while keeping the activation functions same. ANN models with a different number of neurons and their mean squared error values are listed in Table 2. An ANN model with 25 neurons in the hidden layer proved to be the optimum, giving most reasonable correlation between the predicted and measured values, with an MSE value of 0.0117. Figure 7 shows the performance of the neural network during training. As the

validation set was picked at random from a large training set representing wide range of operating points (V, T, L), it is expected that the ANN will generalize well for every case.

**Table 2.** Selection of best performing ANN model based on number of neurons in hidden layer.

Architecture	Neurons in Hidden Layer	Mean Squared Error (MSE)
1	5	0.0185
2	15	0.0124
3	25	0.01176
4	35	0.0134



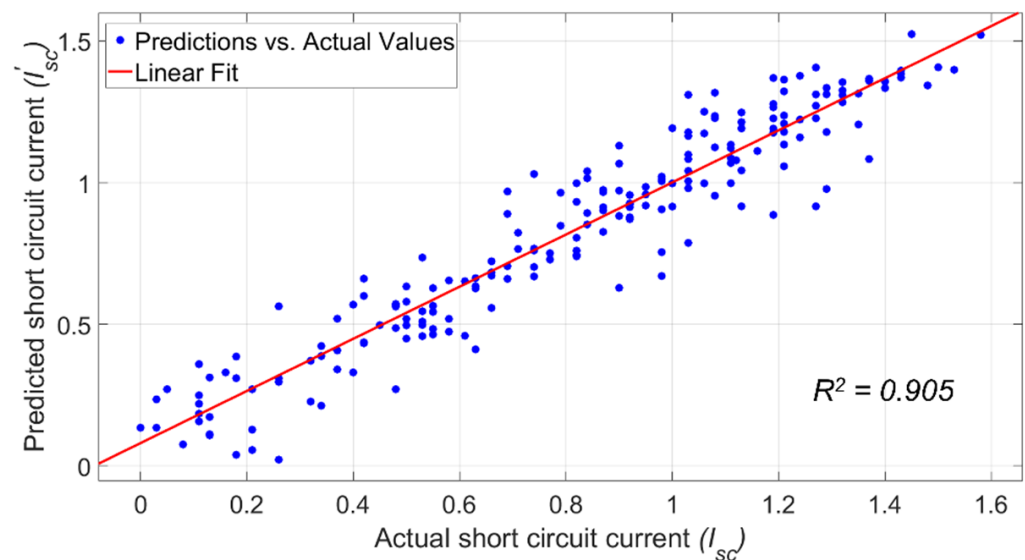
**Figure 7.** ANN's training and validation process.

Figure 8 shows the performance of the ANN model with the test data. The test data provides an unbiased evaluation of the final model fit on training data. As mentioned previously, 20% of the initial dataset was set aside for testing purposes. A coefficient of determination ( $R^2$ ) value of 90.5% was achieved, as shown in Figure 8. This shows that our ANN model does not over-fit and generalizes well for unknown data.

In order to further validate the performance of the ANN model, it was compared with similar soiling detection solutions available in the literature. These techniques involve the use of an ANN model with a single hidden layer for detecting soiling losses in PV [49–51]. These models have been trained on different datasets because of the difference in the nature of input parameters. The detailed performance comparison of above-mentioned techniques with the proposed solution is presented in Table 3. Note that our solution provides better accuracy, with  $R^2$  value of 0.905, as compared to the work of [49,50] and comparable performance to [51], while using least number of input parameters. Ref. [49] uses the daily average values of input parameters such as ambient dust mass concentration, wind speed, and relative humidity. A  $R^2$  value of 0.537 was achieved which is lower than the proposed solution despite using the maximum number of input parameters of all solutions listed in Table 3. Refs. [50,51] use same number of input parameters. Four out of six parameters are same, such as wind velocity, wind direction, temperature, and humidity. Ref. [51] achieved higher value of  $R^2$  (0.928), as compared to  $R^2$ (0.872), achieved by [50]. The difference in  $R^2$  value of can be due to difference of input parameters or the different number of neurons in the hidden layer. The  $R^2$  metric shows that performance achieved by proposed solution is between [50,51], despite using half number of hidden layer neurons.

**Table 3.** Performance comparison of ANN model with different ANN architectures available in the literature.

Parameter	[49]	[50]	[51]	Proposed Model
Hidden layers	1	1	1	1
Neurons in hidden layer	20	10	35	25
Input parameters	10	6	6	3
$R^2$	0.537	0.872	0.928	0.905

**Figure 8.** Real vs. Predicted values of short circuit current after training of ANN on by using unknown dataset.

Besides this, we have used input parameters that are easily available using low-cost sensors. The available literature is mostly focused on presenting solutions for soiling detection without providing practical infrastructure for data communication and observability. Due to the lack of information and communication technology (ICT) infrastructure, the available literature does not provide a complete and scalable solution. Therefore, we have provided a complete solution, in terms of data collection, transmission, and observability, using IoT and cloud computing. The  $SR$  predicted by SCRS and measured soiling ratio ( $SR_m$ ) have been compared in Table 4. The  $SR_m$  value was obtained by using a short circuit current from an actual clean PV panel placed under same environmental conditions as SCRS. The difference between the estimated  $SR$  and measured  $SR$  has been represented in terms of percentage error. Percentage error is calculated according to Equation (6). On average, an error of 4.4% was observed, with 0% and 10.7% being the minimum and maximum values, respectively.

$$Error = \frac{SR_m - SR}{SR_m} \quad (6)$$

**Table 4.** Test results of SCRS, predicted SR is compared to the actual SR to evaluate error.

Plain Data (Soiled Panel)			Normalized Data (Soiled Panel)			$I_{sc}$ (Soiled)	$I'_{sc}$	Estimated SR	Measured SR	Error %
V (volts)	T (°C)	L (lux)	V (volts)	T (°C)	L (lux)					
20.33	62.25	53,084	0.689	0.951	0.678	1	1.19	0.84	0.88	4.5
20.53	61.38	51,609.6	0.705	0.929	0.658	1.06	1.17	0.91	0.89	2.2
20.43	58.5	4,478.76	0.697	0.854	0.569	0.87	1.06	0.82	0.78	5.12
20.43	59.63	37,416.96	0.678	0.883	0.490	0.79	0.97	0.81	0.87	6.8
20.48	55.25	31,334.4	0.702	0.770	0.394	0.74	0.85	0.87	0.88	1.1
20.78	53.38	25,067.52	0.702	0.721	0.312	0.69	0.74	0.93	0.84	10.7
20.58	53.25	19,537.92	0.710	0.718	0.24	0.58	0.6	0.89	0.95	6.3
20.33	48.63	13,455.36	0.689	0.598	0.161	0.37	0.49	0.75	0.77	2.6
21.55	53.00	67,461.13	0.790	0.711	0.865	1.03	1.26	0.82	0.86	4.6
21.16	57.13	64,880.64	0.757	0.818	0.832	1.06	1.27	0.83	0.83	0

## 6. Limitations and Future Work

The SCRS presented in this research uses WiFi technology as a communication channel between the PMC and cloud server. Although WiFi technology allows digital devices to be connected without the need for wires, it is limited in terms of range. If multiple SCRS are deployed at large distances apart, each SCRS system would require a separate WiFi access point. To address this problem, a SCRS data communication architecture with different long range data transfer technology, such as LoRaWAN, is proposed for future research work. LoRaWAN operates on a lower radio frequency band than WiFi; therefore, data can be transferred over long distances without additional costs. LoRaWAN-enabled design will have the following design characteristics.

- SCRS will be equipped with a LoRaWAN transceiver. Each SCRS will transfer data to a central LoRaWAN internet gateway. The gateway will transfer data to the cloud server using a wired or wireless internet connection.
- Using a single gateway as a point of connection between multiple SCRS systems and cloud servers will introduce a single point of failure (SPOF) problem. If the internet gateway device fails, each LoRaWAN-based SCRS will lose its connection to the cloud. To address this issue, a backup gateway device can be added to the network. This backup device will provide an alternate path for the SCRS systems to access the internet and communicate with the cloud server in the case of a failure of the main gateway device.
- Edge intelligence can be improved further by adding context awareness. Data from a SCRS system will be transferred by gateway if it differs from the previous data by a certain amount, therefore reducing the redundancies in the data transfer. This will help to conserve the channel bandwidth between the gateway and cloud server.

## 7. Conclusions

PV plants vary in terms of the number of PV arrays and amount of area covered. This means that multiple soiling stations are required for larger installations, and a simplified low-cost solution is required for small-scale deployments. In this research, a new method, "SCRS", was proposed for the detection of soiling losses in PV plants. A cloud-based IoT infrastructure was proposed, where the ANN algorithm was hosted on a centralized cloud server. SCRS used an ANN model with single hidden layer to estimate the soiling ratio. The ANN algorithm was trained successfully, with a mean squared error of 0.0117. The proposed ANN model was also compared to another model present in the literature. We proposed a complete scalable solution for the detection of soiling losses. The main role of the soiling station was to collect the electrical and environmental parameters. The parameters were transmitted to the cloud server using the IoT communication protocol (MQTT). The ANN model was implemented in the cloud server to detect the soiling ratio, and the results were transmitted to the graphical user interface. The integration of IoT-based communication provided the added benefit of eliminating the wiring required from soiling stations to monitoring station, as data could be transmitted wirelessly through the internet. A test dataset was used to validate the performance of SCRS. An adjusted

R-squared ( $R^2$ ) value of 0.905 was achieved on the test data. Furthermore, the estimated soiling ratio from SCRS was compared to the actual soiling ratio to calculate the percentage error. The average, maximum, and minimum values of percentage error were found to be 4.33, 10.7, and 0, respectively.

**Author Contributions:** Conceptualization, M.U.M. and A.U.; methodology, M.U.M. and A.U.; software, M.U.M. and A.U.; validation, M.U.M., A.U., H.S.Z. and W.A.; formal analysis, W.U. and A.U.; investigation, A.U., K.Z. and W.U.; resources, A.U., W.U. and H.-J.K.; data curation, M.U.M. and A.U.; writing—original draft preparation, M.U.M. and A.U.; writing—review and editing, M.U.M., A.U., H.-J.K. and W.U.; visualization, A.U. and H.S.Z.; supervision, A.U.; project administration, A.U.; funding acquisition, A.U. and W.U. All authors have read and agreed to the published version of the manuscript.

**Funding:** This research received no external funding.

**Data Availability Statement:** Not applicable.

**Conflicts of Interest:** There is no conflict of interest.

### Abbreviations

The following abbreviations are used in this manuscript:

SCRS	Solar Conversion Recovery System
IoT	Internet of Things
ANN	Artificial Neural Network
MSE	Mean Squared Error
MQTT	Message Queuing Telemetry Transport
PV	Photovoltaic
AI	Artificial Intelligence
HTTP	Hypertext Transfer Protocol
PMC	Performance Measurement Cabinet
SR	Soiling Ratio
RTC	Real Time Clock
ADC	Analog to Digital Converter
JSON	JavaScript Object Notation

### References

1. Marks-Bielska, R.; Bielski, S.; Pik, K.; Kurowska, K. The importance of renewable energy sources in Poland's energy mix. *Energies* **2020**, *13*, 4624. [[CrossRef](#)]
2. Siddique, H.M.A.; Kiani, A.K. Industrial pollution and human health: evidence from middle-income countries. *Environ. Sci. Pollut. Res.* **2020**, *27*, 12439–12448. [[CrossRef](#)]
3. Martins, F.; Felgueiras, C.; Smitkova, M.; Caetano, N. Analysis of fossil fuel energy consumption and environmental impacts in European countries. *Energies* **2019**, *12*, 964. [[CrossRef](#)]
4. Qiu, T.; Wang, L.; Lu, Y.; Zhang, M.; Qin, W.; Wang, S.; Wang, L. Potential assessment of photovoltaic power generation in China. *Renew. Sustain. Energy Rev.* **2022**, *154*, 111900. [[CrossRef](#)]
5. Zekry, A.; Shaker, A.; Salem, M. *Solar Cells and Arrays: Principles, Analysis, and Design*; Elsevier: Amsterdam, The Netherlands, 2018; pp. 3–56.
6. Naceur, F.B.; Salah, C.B.; Telmoudi, A.J.; Mahjoub, M.A. Intelligent approach for optimal sizing in photovoltaic panel-battery system and optimizing smart grid energy. *Trans. Inst. Meas. Control* **2021**. [[CrossRef](#)]
7. Javed, W.; Guo, B.; Figgis, B.; Pomares, L.M.; Aissa, B. Multi-year field assessment of seasonal variability of photovoltaic soiling and environmental factors in a desert environment. *Sol. Energy* **2020**, *211*, 1392–1402. [[CrossRef](#)]
8. Song, Z.; Liu, J.; Yang, H. Air pollution and soiling implications for solar photovoltaic power generation: A comprehensive review. *Appl. Energy* **2021**, *298*, 117247. [[CrossRef](#)]
9. Costa, S.C.; Diniz, A.S.A.; Kazmerski, L.L. Solar energy dust and soiling R&D progress: Literature review update for 2016. *Renew. Sustain. Energy Rev.* **2018**, *82*, 2504–2536.
10. Shaju, A.; Chacko, R. Soiling of photovoltaic modules-Review. In Proceedings of the IOP Conference Series: Materials Science and Engineering, Kerala State, India, 20–21 April 2018; Volume 396, p. 012050.
11. Bessa, J.G.; Micheli, L.; Almonacid, F.; Fernández, E.F. Monitoring photovoltaic soiling: Assessment, challenges, and perspectives of current and potential strategies. *Iscience* **2021**, *24*, 102165. [[CrossRef](#)]

12. Paudyal, B.R.; Shakya, S.R.; Paudyal, D.P.; Das Mulmi, D. Soiling-induced transmittance losses in solar PV modules installed in Kathmandu Valley. *Renew. Wind Water Solar* **2017**, *4*, 1–8. [CrossRef]
13. Schill, C.; Brachmann, S.; Koehl, M. Impact of soiling on IV-curves and efficiency of PV-modules. *Sol. Energy* **2015**, *112*, 259–262. [CrossRef]
14. Cordero, R.; Damiani, A.; Laroze, D.; MacDonell, S.; Jorquera, J.; Sepúlveda, E.; Feron, S.; Llanillo, P.; Labbe, F.; Carrasco, J.; et al. Effects of soiling on photovoltaic (PV) modules in the Atacama Desert. *Sci. Rep.* **2018**, *8*, 1–14. [CrossRef]
15. Figgis, B.; Ennaoui, A.; Ahzi, S.; Rémond, Y. Review of PV soiling measurement methods. In Proceedings of the 2016 International Renewable and Sustainable Energy Conference (IRSEC), Marrakech, Morocco, 14–17 November 2016; pp. 176–180.
16. Costa, S.C.; Kazmerski, L.L.; Diniz, A.S.A. Estimate of Soiling Rates Based on Soiling Monitoring Station and PV System Data: Case Study for Equatorial-Climate Brazil. *IEEE J. Photovoltaics* **2021**, *11*, 461–468. [CrossRef]
17. Yang, M.; Ji, J.; Guo, B. Soiling Quantification Using an Image-Based Method: Effects of Imaging Conditions. *IEEE J. Photovoltaics* **2020**, *10*, 1780–1787. [CrossRef]
18. Tribak, H.; Zaz, Y. Dust Soiling Concentration Measurement on Solar Panels based on Image Entropy. In Proceedings of the 2019 7th International Renewable and Sustainable Energy Conference (IRSEC), Agadir, Morocco, 27–30 November 2019; pp. 1–4.
19. Kintech-Engineering. SOILING MEASUREMENT UNIT. Available online: [https://www.kintech-engineering.com/catalogue/soiling-measurement-kit/soiling-measurement-kit/#ywtm\\_438](https://www.kintech-engineering.com/catalogue/soiling-measurement-kit/soiling-measurement-kit/#ywtm_438) (accessed on 4 October 2022).
20. NRGSystems. SRA System. Available online: <https://www.nrgsystems.com/products/solar/detail/sra-system/> (accessed on 4 October 2022).
21. Gostein, M.; Düster, T.; Thuman, C. Accurately measuring PV soiling losses with soiling station employing module power measurements. In Proceedings of the 2015 IEEE 42nd Photovoltaic Specialist Conference (PVSC), Washington, DC, USA, 25–30 June 2017; pp. 1–4.
22. Gupta, V.; Sharma, M.; Pachauri, R.K.; Babu, K.D. A low-cost real-time IOT enabled data acquisition system for monitoring of PV system. *Energy Sources Part Recover. Util. Environ. Eff.* **2021**, *43*, 2529–2543. [CrossRef]
23. Kazmi, S.N.A.; Ulasayar, A.; Khan, M.F.N. IoT based energy efficient smart street lighting technique with air quality monitoring. In Proceedings of the 2020 14th International Conference on Open Source Systems and Technologies (ICOSST), Lahore, Pakistan, 16–17 December 2020; pp. 1–6.
24. Ashfaq, Q.; Ulasayar, A.; Zad, H.S.; Khattak, A.; Imran, K. Hour-ahead global horizontal irradiance forecasting using long short term memory network. In Proceedings of the 2020 IEEE 23rd International Multitopic Conference (INMIC), Lahore, Pakistan, 16–17 December 2020; pp. 1–6.
25. Kazmi, S.N.A.; Ulasayar, A.; Khattak, A.; Zad, H.S. A new state of charge estimation technique of lithium-ion battery using adaptive extended Kalman filter and artificial neural network. *Trans. Inst. Meas. Control* **2022**. [CrossRef]
26. Ali, W.; Ulasayar, A.; Mehmood, M.U.; Khattak, A.; Imran, K.; Zad, H.S.; Nisar, S. Hierarchical control of microgrid using IoT and machine learning based islanding detection. *IEEE Access* **2021**, *9*, 103019–103031. [CrossRef]
27. Ghasempour, A. Internet of things in smart grid: Architecture, applications, services, key technologies, and challenges. *Inventions* **2019**, *4*, 22. [CrossRef]
28. Li, B.; Delpha, C.; Diallo, D.; Migan-Dubois, A. Application of Artificial Neural Networks to photovoltaic fault detection and diagnosis: A review. *Renew. Sustain. Energy Rev.* **2021**, *138*, 110512. [CrossRef]
29. Üstün, İ.; Üneş, F.; Mert, İ.; Karakuş, C. A comparative study of estimating solar radiation using machine learning approaches: DL, SMGRT, and ANFIS. *Energy Sources Part Recover. Util. Environ. Eff.* **2020**, 10322–10345. [CrossRef]
30. Khan, S.U.; Khan, N.; Ullah, F.U.M.; Kim, M.J.; Lee, M.Y.; Baik, S.W. Towards Intelligent Building Energy Management: AI-based Framework for Power Consumption and Generation Forecasting. *Energy Build.* **2022**, *279*, 112705. [CrossRef]
31. Khan, N.; Ullah, F.U.M.; Haq, I.U.; Khan, S.U.; Lee, M.Y.; Baik, S.W. AB-net: A novel deep learning assisted framework for renewable energy generation forecasting. *Mathematics* **2021**, *9*, 2456. [CrossRef]
32. Mohammadian, V.; Navimipour, N.J.; Hosseinzadeh, M.; Darwesh, A. Comprehensive and systematic study on the fault tolerance architectures in cloud computing. *J. Circuits, Syst. Comput.* **2020**, *29*, 2050240. [CrossRef]
33. Aliwarga, H.K.; Satriatama, A.H.; Pratama, B.F.A. Performance comparison of fleet management system using IoT node device based on MQTT and HTTP protocol. *AIP Conf. Proc.* **2020**, 2217, 020009.
34. Wukkadada, B.; Wankhede, K.; Nambiar, R.; Nair, A. Comparison with HTTP and MQTT in Internet of Things (IoT). In Proceedings of the 2018 International Conference on Inventive Research in Computing Applications (ICIRCA), Coimbatore, India, 11–12 July 2018; pp. 249–253.
35. Sutikno, T.; Purnama, H.S.; Pamungkas, A.; Fadlil, A.; Alsofyani, I.M.; Jopri, M.H. Internet of things-based photovoltaics parameter monitoring system using NodeMCU ESP8266. *Int. J. Electr. Comput. Eng.* **2021**, *11*. [CrossRef]
36. Ul Mehmood, M.; Ulasayar, A.; Khattak, A.; Imran, K.; Sheh Zad, H.; Nisar, S. Cloud based iot solution for fault detection and localization in power distribution systems. *Energies* **2020**, *13*, 2686. [CrossRef]
37. Lachhab, F.; Bakhouya, M.; Ouladsine, R.; Essaaidi, M. A context-driven platform using Internet of things and data stream processing for heating, ventilation and air conditioning systems control. *Proc. Inst. Mech. Eng. Part J. Syst. Control. Eng.* **2019**, *233*, 877–888. [CrossRef]

38. Lachhab, F.; Bakhouya, M.; Ouladsine, R.; Essaaidi, M. Context-driven monitoring and control of buildings ventilation systems using big data and Internet of Things—Based technologies. *Proc. Inst. Mech. Eng. Part J. Syst. Control. Eng.* **2019**, *233*, 276–288. [[CrossRef](#)]
39. Al-Masri, E.; Kalyanam, K.R.; Batts, J.; Kim, J.; Singh, S.; Vo, T.; Yan, C. Investigating messaging protocols for the Internet of Things (IoT). *IEEE Access* **2020**, *8*, 94880–94911. [[CrossRef](#)]
40. Nakabi, T.A.; Toivanen, P. An ANN-based model for learning individual customer behavior in response to electricity prices. *Sustain. Energy Grids Netw.* **2019**, *18*, 100212. [[CrossRef](#)]
41. Chettibi, N.; Pavan, A.M.; Mellit, A.; Forsyth, A.; Todd, R. Real-time prediction of grid voltage and frequency using artificial neural networks: An experimental validation. *Sustain. Energy, Grids Netw.* **2021**, *27*, 100502. [[CrossRef](#)]
42. Abdullah, H.M.; Kamel, R.M.; El-Sayed, M. Non-communication and artificial neural network based photovoltaic monitoring using the existing impedance relay. *Sustain. Energy Grids Netw.* **2020**, *22*, 100335. [[CrossRef](#)]
43. Ding, B.; Qian, H.; Zhou, J. Activation functions and their characteristics in deep neural networks. In Proceedings of the 2018 Chinese control and decision conference (CCDC), Shenyang, China, 9–11 June 2018; pp. 1836–1841.
44. Wao, A.A.; Soni, B.K. Performance Analysis of Sigmoid and Relu Activation Functions in Deep Neural Network. In *Intelligent Systems*; Springer: Berlin/Heidelberg, Germany, 2021; pp. 39–52.
45. De Villiers, J.; Barnard, E. Backpropagation neural nets with one and two hidden layers. *IEEE Trans. Neural Netw.* **1993**, *4*, 136–141. [[CrossRef](#)]
46. Biswas, S.K.; Chakraborty, M.; Singh, H.R.; Devi, D.; Purkayastha, B.; Das, A.K. Hybrid case-based reasoning system by cost-sensitive neural network for classification. *Soft Comput.* **2017**, *21*, 7579–7596. [[CrossRef](#)]
47. Shanker, M.; Hu, M.Y.; Hung, M.S. Effect of data standardization on neural network training. *Omega* **1996**, *24*, 385–397. [[CrossRef](#)]
48. Ghaedi, A.; Ghaedi, M.; Pouranfard, A.; Ansari, A.; Avazzadeh, Z.; Vafaei, A.; Tyagi, I.; Agarwal, S.; Gupta, V.K. Adsorption of Triamterene on multi-walled and single-walled carbon nanotubes: Artificial neural network modeling and genetic algorithm optimization. *J. Mol. Liq.* **2016**, *216*, 654–665. [[CrossRef](#)]
49. Javed, W.; Guo, B.; Figgis, B. Modeling of photovoltaic soiling loss as a function of environmental variables. *Sol. Energy* **2017**, *157*, 397–407. [[CrossRef](#)]
50. Zitouni, H.; Azouzoute, A.; Hajjaj, C.; El Ydrissi, M.; Regragui, M.; Polo, J.; Oufadel, A.; Bouaichi, A.; Ghennioui, A. Experimental investigation and modeling of photovoltaic soiling loss as a function of environmental variables: A case study of semi-arid climate. *Sol. Energy Mater. Sol. Cells* **2021**, *221*, 110874. [[CrossRef](#)]
51. Laarabi, B.; Tzuc, O.M.; Dahlioui, D.; Bassam, A.; Flota-Bañuelos, M.; Barhdadi, A. Artificial neural network modeling and sensitivity analysis for soiling effects on photovoltaic panels in Morocco. *Superlattices Microstruct.* **2019**, *127*, 139–150. [[CrossRef](#)]

**Disclaimer/Publisher’s Note:** The statements, opinions and data contained in all publications are solely those of the individual author(s) and contributor(s) and not of MDPI and/or the editor(s). MDPI and/or the editor(s) disclaim responsibility for any injury to people or property resulting from any ideas, methods, instructions or products referred to in the content.